Plasmonics (2025) 20:4577–4587
https://doi.org/10.1007/s11468-024-02500-4

RESEARCH

Sensitivity Enhancement by the Ag/Few-Layer Black Phosphorus/Mxene Structure in Surface Plasmon Resonance Biochemical Sensor

Jingwei Lv[1] · Ying Yu[1] · Chao Mi[2] · Debao Wang[1] · Wei Li[1] · Yanru Ren[1] · Jianxin Wang[1] · Wei Liu[1] · Paul K. Chu[3,4,5] · Chao Liu[1]

Received: 14 July 2024 / Accepted: 16 August 2024 / Published online: 18 November 2024

Abstract

A highly sensitive surface plasmon resonance biosensor composed of the hybrid black phosphorus-MXene ($Ti_3C_2T_x$) structure and Ag bimetal layers is designed and investigated analytically by the angular interrogation technique. The use of bilayer Ag enhances the sensitivity compared to a single metal layer. Black phosphorus enhances the light-matter interaction due to its layer-dependent direct and tunable bandgap. The thickness of the BP and Ag layers and the number of $Ti_3C_2T_x$ sheets are optimized to maximize the sensitivity. It covers a wide range of refractive index (RI) from 1.330 to 1.335, for which an optimized angular sensitivity of 450°/RIU is observed from the Ag bimetal MXene-based SPR biosensor. It can be fabricated as a sensor chip for efficient sensing of analytes or biochemical molecules by carefully controlling the surface termination of $Ti_3C_2T_x$. The encouraging results from this research underscore the high potential of this structure in surface plasmon resonance biosensors, which is crucial for the early detection of biological diseases. By overcoming the limitations of traditional sensors, this innovative structure boasts both high sensitivity and rapid response speed, thereby demonstrating the remarkable potential for market adoption and application in biomedical research, ultimately enhancing the effectiveness of disease treatment through earlier interventions.

Keywords Black phosphorus · MXene · Angular interrogation · Surface plasmon resonance · Sensitivity

Introduction

Recently, the promotion of interactions between biological analytes and detection platforms for the purpose of flexible detection has become a hot research topic in the field of biotechnology [3–7]. Optical biosensors based on the surface plasmon resonance (SPR) effect have gained widespread popularity in various applications, including drug discovery, enzyme detection, and medical diagnosis [2, 50]. Surface plasmons (SPPs) are electron-density oscillations occurring at the interface between a metal and dielectric characterized by negative and positive permittivity, respectively [6, 8–11]. In SPR biosensors, the reversible adsorption of biomolecules (analyte) on the sensing surface (metal/dielectric interface) alters the local refractive index (RI) and the SPR condition.

SPR biosensors can be categorized into two prism coupling types, Otto and Kretschmann configurations. Both configurations operate based on the angular interrogation technique. The Kretschmann configuration is simple and produces a high signal-to-noise ratio (SNR) with single radiation. In traditional SPR sensors, metallic materials such as silver (Ag), gold (Au), aluminum (Al), and copper (Cu) are employed to produce the plasmonic effects for sensing [11–14]. Recently, 2D materials such as graphene, MoS_2, and black phosphorous (BP) have been proposed for SPR biosensors [15, 25, 27–29,] because 2D materials can enhance the sensitivity. MXene

✉ Chao Liu
msm-liu@126.com

1 School of Physics and Electronic Engineering, Northeast Petroleum University, Daqing 163318, China

2 Digital Intelligence Technology Company, Daqing Oilfield, Daqing 163453, China

3 Department of Physics, City University of Hong Kong, Tat Chee Avenue, Kowloon, Hong Kong, China

4 Department of Materials Science and Engineering, City University of Hong Kong, Tat Chee Avenue, Kowloon, Hong Kong, China

5 Department of Biomedical Engineering, City University of Hong Kong, Tat Chee Avenue, Kowloon, Hong Kong, China

($Ti_3C_2T_x$) contains functional groups making it suitable for the detection of certain analytes [31–33]. Wu et al. have designed an SPR biosensor by increasing the BP layer to enhance the sensitivity caused by light absorption of graphene [14]. The sensitivity increases to a maximum of 217°/RIU when the number of graphene layers is 5. Singh et al. have designed an SPR chemical sensor with black phosphorus and graphene together with a gold bilayer for enhanced sensitivity [44]. Mudgal et al. have proposed a highly sensitive SPR biosensor based on silver (Ag), barium titanate (BaTiO3), graphene, and affinity layer for the detection of Pseudomonas bacteria [49].

Black phosphorous (BP) is an allotrope of phosphorus having a honeycomb lattice structure bounded covalently within the layer through van der Waals forces. The structure provides easy exfoliation of thin phosphorene layers. BP possesses a direct and tunable band gap ranging from 0.3 eV (bulk) to 2 eV (monolayer), making it highly versatile for electronic and optoelectronic device applications[16, 17]. In addition, the direction-dependent crystallographic structure of BP results in the anisotropic behavior which makes BP quite useful for direction-dependant applications [20]. BP's biocompatibility also opens the possibilities for its uses for the applications in biomedicine such as drug delivery. MXene is an emerging two-dimensional material known for its unique physiochemical characteristics and ultrathin structures, surpassing graphene and other 2D materials. MXene is more advantageous than other 2D materials due to its two main properties: metallic nature and hydrophilicity [32, 33]. MXene is used in SPR because it increases the biomolecule adsorption rate and prevents the metal layer from oxidation. These characteristics make them promising candidates for exemplary performance in biosensing devices.

The hybrid structure of BP and MXene ($Ti_3C_2T_x$) can be used in the SPR sensor to enhance the sensing properties for adsorbed analytes due to the functionalized surface of $Ti_3C_2T_x$ and enhanced light-matter interactions rendered by BP [1, 29, 31]. Their high success rate in detecting bacteria, DNA, viruses, antibodies, lipids, peptides, and ions [22, 22, 24, 33] encourages us to undertake Pseudomonas bacteria detection in this study. The affinity layer is placed just below the sensing medium. It bonds with Pseudomonas bacteria [52]. Many Pseudomonas bacteria were attached to the affinity layer for carbon sources such as toluene and nicotine. The adhesion of Pseudomonas bacteria to hydrophilic metals was studied. When the sensor is exposed to different analytes for detection, the physical properties of the material at the end of the sensor, such as hydrophilic ability and molecular absorption capacity, can be utilized to achieve interaction between the sensor and the analyte. This enables the acquisition of offset resonance curves for analytes with different refractive indices, achieving the purpose of detection and identification.

After vertically stacking different 2D-layered materials together, van der Waals heterostructures (vdWh) and superlattices are formed. These structures can manipulate optical and electronic properties based on the interaction between their layers, allowing for the development of next-generation devices. Herein, the hybrid prism biochemical sensor consisting of low refractive index CaF_2, bilayer metallic silver[43], and 2D materials black phosphorus and MXene ($Ti_3C_2T_x$) is designed, and the SPR sensor based on the Kretschmann configuration is numerically analyzed under visible-light irradiation by angular interrogation, which is designed to stimulate surface plasmon resonance to enhance the sensitivity. The proposed SPR biosensor performance is realized theoretically through COMSOL software. By optimizing the structural parameters, the best sensitivity is attained from the structure with nine layers of black phosphorus and 7-nm-thick silver. The best sensitivity at 662 nm is 450°/RIU, which is 3.9 and 2.5 times higher than that of the prismatic sensors based on Ag-BP structures and conventional single-layer metal, respectively. Our results provide insights into the excitation of SPR and the development of biochemical sensors with enhanced sensitivity.

Design and Theoretical Model

The SPR biochemical sensor composed of few-layer BP-MXene is depicted schematically in Fig. 1. In this structure, CaF_2 glass (np = 1.43286 at $\lambda = 662$ nm) is chosen for the coupling prism, and the 40-nm-thick silver (Ag) metal film excites SPP.

According to the Drude model, the dielectric constant of Ag can be determined by Eq. (1) [40]:

$$n_m = \sqrt{\varepsilon_m} = \left[1 - \frac{\lambda^2 \lambda_c}{\lambda_p^2(\lambda_c + i\lambda)}\right]^{1/2}, \quad (1)$$

where λ_p and λ_c represent the plasma and collision wavelengths, and the values of λ_p and λ_c for Ag are 1.4541×10^{-7} m and 1.7614×10^{-5} m, respectively.

Black phosphorus (BP), as a promising new 2D material, joined the 2D material family since 2014 and has rapidly attracted significant attentions due to its widely tunable and direct bandgap, high carrier mobility, and remarkable electrical, optical, and phonon properties [25, 26, 41]. However, BP is a readily oxidizable material in ambient conditions which needs a protective layer to prevent it from oxidation. Here, we chose Ag to be coated on BP as a protective layer to compensate for its easy oxidative volatilization and further improve sensitivity. Therefore, the sensor structure of this design is coated with a few layers of BP (5.85 nm, containing nearly nine layers) which is coated on the Ag film, and an Ag layer is deposited on the few-layer BP to prevent oxidation. The fifth layer is $Ti_3C_2T_x$

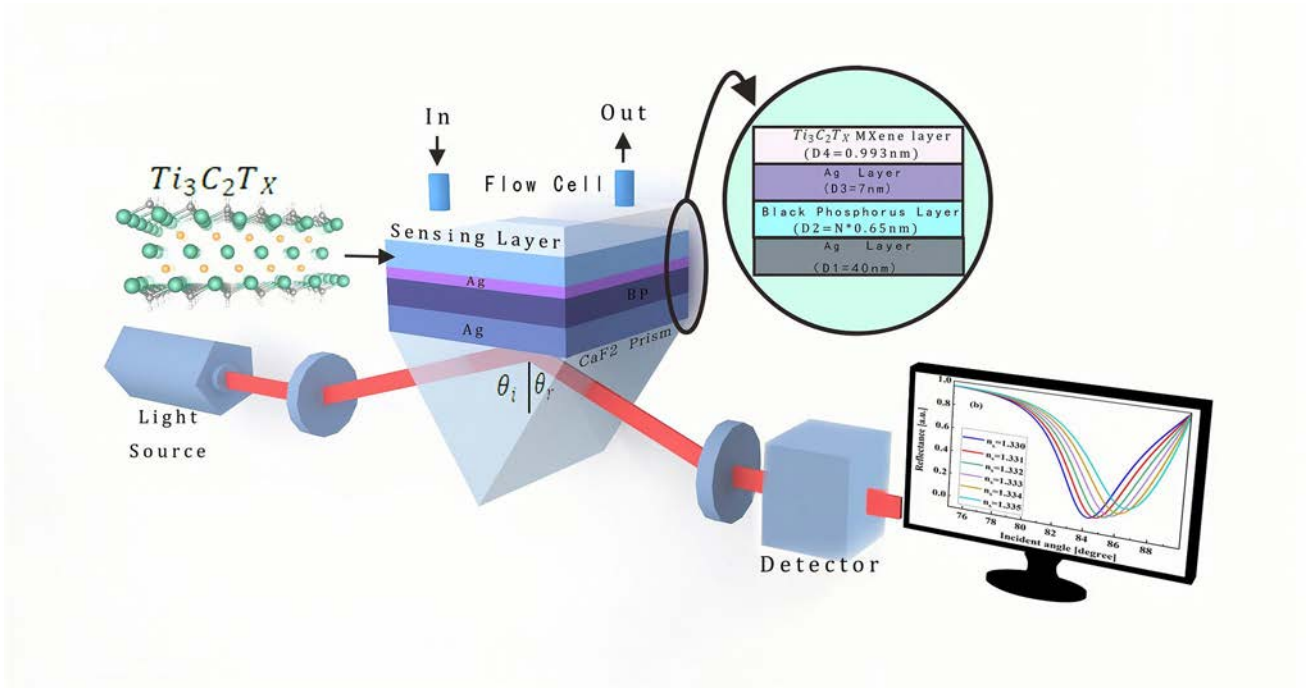

Fig. 1 Schematic diagram of the SPR sensor and detection setup

with a refractive index (RI) of 2.38 + 1.33i on the Ag layer to avoid the oxidation of Ag [30, 34]. The $Ti_3C_2T_x$ layer deposited on Ag as the BRE layer can be used to sense biochemical molecules and analytes [41]. The hydrophilic functional group (i.e., –OH, –O, –F) on $Ti_3C_2T_x$ captures water molecules for detecting biochemical molecules in an aqueous solution with enhanced sensitivity [19]. At the same time, the layered $Ti_3C_2T_x$ has a larger surface area allowing the attachment of more biochemical molecules/analytes. The thickness and refractive index of the sensor at λ = 662 nm are shown in Table 1.

Enzymes, proteins, and DNA can be detected. The sensing medium is the last layer, and in an aqueous solution, the RI is $1.33+\Delta n_{SM}$, where $\Delta n_{SM}=0.005$ is the RI shift due to analyte adsorption on $Ti_3C_2T_x$ [19, 41]. The RI range is between 1.330 and 1.335, attributable to variations in the mass ratios of solutes in the phosphate buffer saline (PBS) solution [19]. The reflectivity of the multilayer structure is derived by Eq. (2) [41]:

$$r_{pm_1d_1m_2d_2}=\frac{r_{pm_1}+r_{m_1d_1m_2d_2}e^{2iK_{m_1xd_{m_1}}}}{1+r_{pm_1}r_{m_1d_1m_2d_2}e^{2iK_{m_1xd_{m_1}}}}, \tag{2}$$

and

$$K_{ix}=\sqrt{(\frac{2\pi}{\lambda})^2\varepsilon_i-K_Z^2};i=p,m_1,d_1,m_2,d_2 \tag{3}$$

$$r_{pm}=\frac{\left(\varepsilon_mK_{px}-\varepsilon_pK_{mx}\right)}{\left(\varepsilon_mK_{px}+\varepsilon_pK_{mx}\right)};r_{md}=\frac{\left(\varepsilon_dK_{mx}-\varepsilon_mK_{dx}\right)}{\left(\varepsilon_dK_{mx}+\varepsilon_mK_{dx}\right)}, \tag{4}$$

where p, m, and d denote the prism, metal, and dielectrics, respectively.

The resonance dip in the reflectance curve occurs when the resonance condition is satisfied, as shown by Eq. (2). Therefore, the coupling equation for incident light and SPs at the metal–dielectric interface can be derived from Eq. (2) as follows:

$$k_z=k_{sp}=\frac{2\pi}{\lambda}n_p\sin\theta_{spr}=real(\frac{2\pi}{\lambda}\sqrt{\frac{\varepsilon_m\varepsilon_s}{\varepsilon_m+\varepsilon_s}}) \tag{5}$$

In Eq. (5), n_p is the RI of the substrate (glass/prism), and λ is the wavelength. The dielectric constants of the metal layer and sensing (analyte) layers are ε_m and ε_s, respectively. The

Table 1 Thickness and refractive index of sensors at $\lambda = 662$ nm

Layers	Materials	Refractive index ($\lambda = 662$ nm)		Thickness (nm)	Ref
		Real (n)	Imaginary (k)		
I	Prism CaF_2	1.43286	—	—	[21]
II	Metal Ag	0.04944	4.5027	40	[41]
III	2D material BP	3.8337	0.015215	0.65	[1]
IV	Metal Ag	0.04944	4.5027	7	[41]
V	Mxene $Ti_3C_2T_x$			0.993	[42]

angle at which the SPR curve dips (R_{min}) is the resonance angle (SPR angle), which occurs due to the transition in the RI of the analyte.

A comparative analysis of several prisms [21] in terms of the reflectance curves indicates that the CaF_2 prism has the largest SPR angle, and it is chosen as a light coupling glass at 662 nm. The structure consists of layers of Ag, BP, Ag, and $Ti_3C_2T_x$ on top of the coupling prism, with Ag serving as the SPR-active metal layer. $Ti_3C_2T_x$ is considered the last layer that interacts directly with the analyte. The dielectric constants of $Ti_3C_2T_x$, Ag, CaF_2, and BP at 662 nm are extracted from Refs. [44–46].

The essential sensor characteristic, sensitivity, illustrates how the resonance angle changes in response to the sensing medium's RI changes. Its value should be greater for the SPR sensor. The sensitivity (S) is calculated by Eq. (6) [44]:

$$S = \frac{\Delta\theta_{SPR}}{\Delta n_S}, \tag{6}$$

The figure of merit (FOM) is an important index to analyze the comprehensive properties of sensors according to Eq. (7) [47]:

$$FOM = \frac{S}{FWHM}, \tag{7}$$

Detection accuracy (D.A.) is the reciprocal of the FWHM [48]. Signal-to-noise ratio (SNR) and detection limit (DL) are also considered important performance parameters [47]. SNR is used to measure the ratio of signal to noise, with higher SNR indicating better performance of the sensor. DL represents the lowest amount of analyte that can be reliably detected by the proposed sensor, with a preference for smaller values [47]. The D.A., SNR, and DL of the sensor have been investigated [44, 47, 51] and calculated as:

$$DA = \frac{1}{FWHM}, \tag{8}$$

$$SNR = \frac{\Delta\theta_{SPR}}{FWHM}, \tag{9}$$

$$DL = \frac{\Delta n_S}{\Delta\theta_{SPR}} \times 0.001^{\circ}. \tag{10}$$

Fabrication Steps

The possible fabrication steps have been shown here step by step and can be illustrated in Fig. 2.

The proposed SPR sensor is composed of a multilayer structure based on the Kretschmann configuration. The layers of Ag, BP, and $Ti_3C_2T_x$ may be deposited by physical vapor deposition (PVD) [49], chemical vapor deposition (CVD), and plasma fluorination.

Finally, a sensing medium has been established for the analyte-biochemical molecules interaction. After the manufacturing process, the SPR chip is placed above the prism, and experimental calculations are found using the SPR sensor setup.

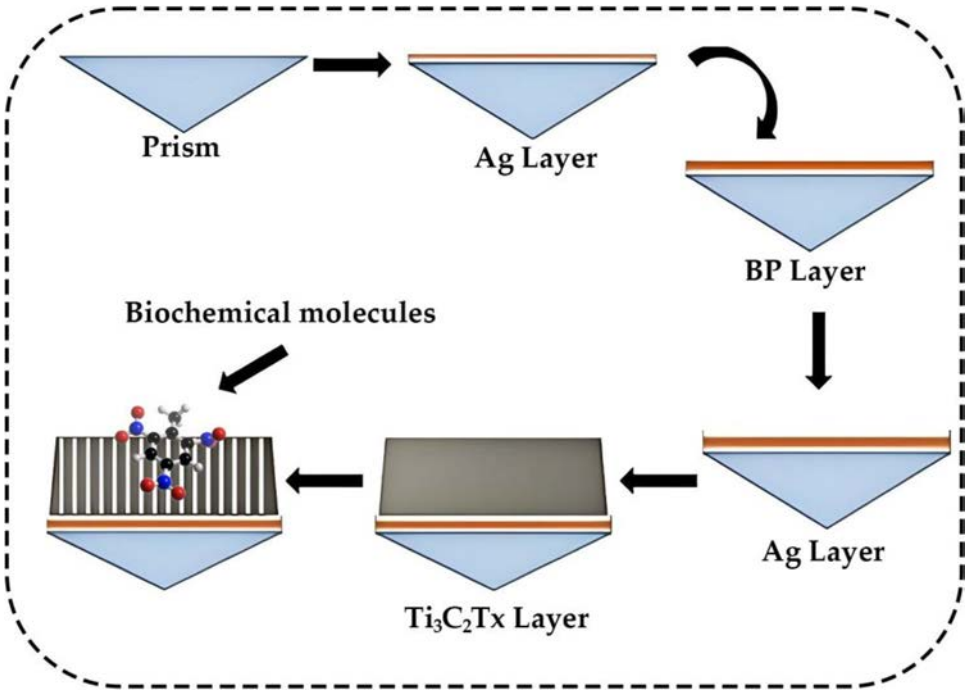

Fig. 2 Schematic diagram of the manufacturing steps of the proposed sensor

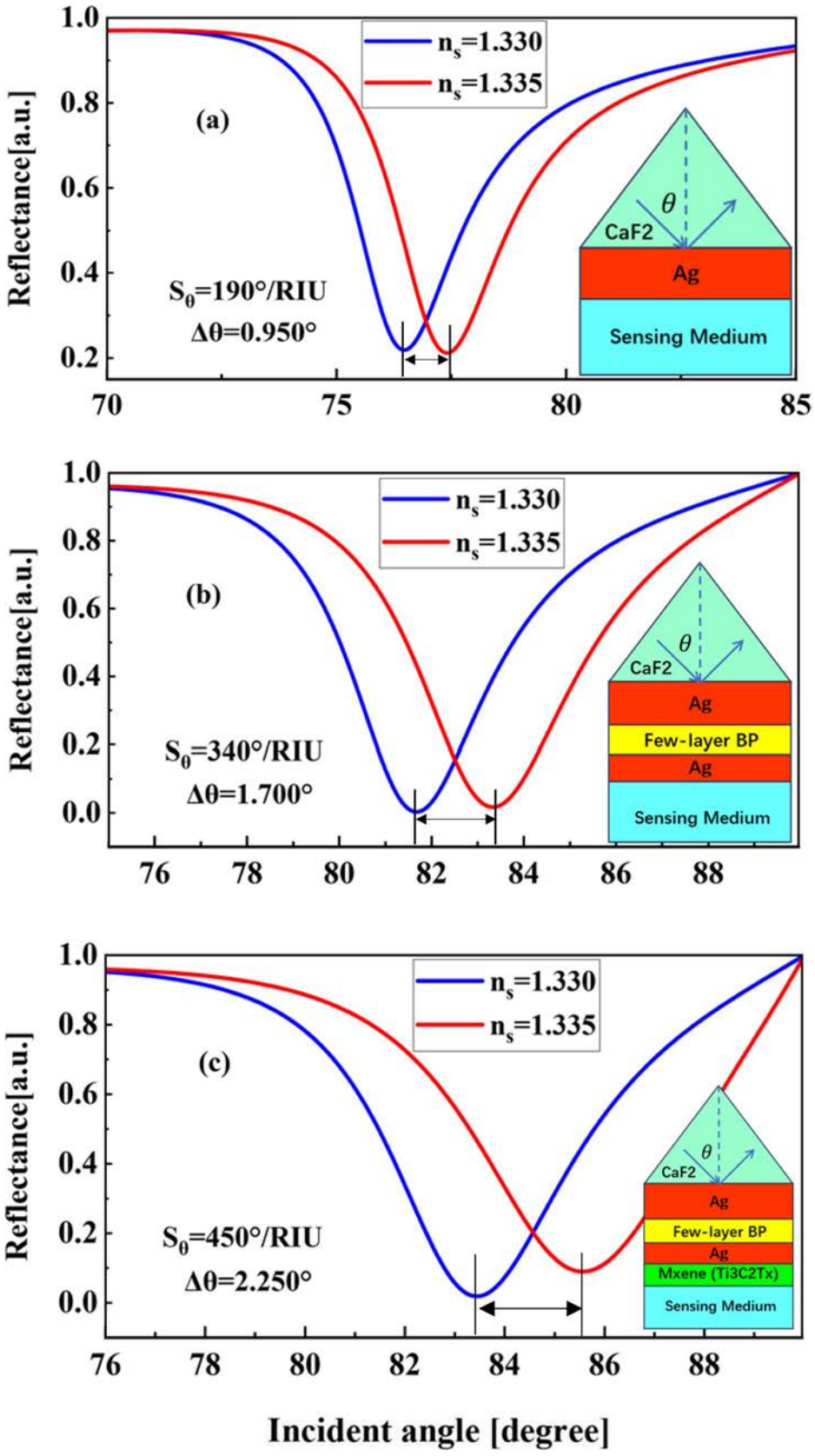

Fig. 3 Variation of the reflectance with respect to the incident angle: **a** conventional biochemical sensor with a single Ag film, **b** biochemical sensor with two Ag—5.85-nm-thick few-layer BP, and **c** biochemical sensor with the 5-nm-thick BP—$Ti_3C_2T_x$ heterostructure

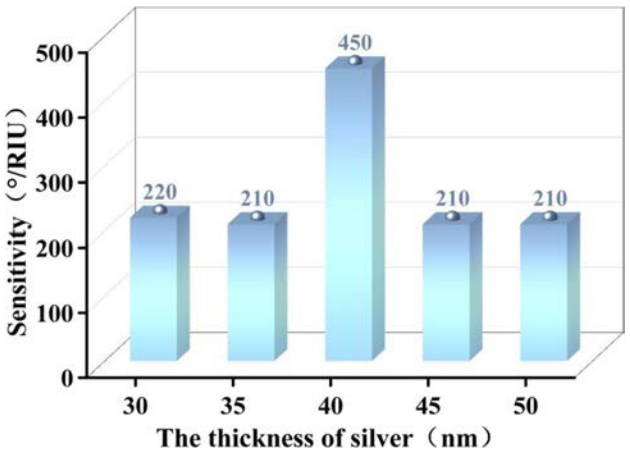

Fig. 4 Sensitivity of the first layer of silver at different thicknesses

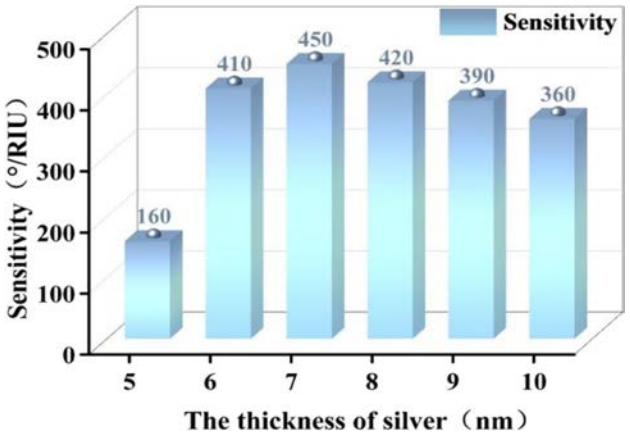

Fig. 5 Sensitivity of silver layers with different thicknesses

Results and Discussion

The coupling prism is made of CaF_2 because the relatively low RI can improve the sensitivity. The reflectance graphs as a function of the incident angle are acquired from the single-layer and multilayer sensors, as shown in Fig. 3. The schematic of the traditional SPR biochemical sensor based on the Kretschmann geometry comprising the sensing medium, Ag layer, and CaF_2 (shown in insets) is shown in Fig. 3a. As the RI of the sensing medium varies from $n = 1.330$ to 1.335, red-shifting is observed from the reflectance spectra [1]. The sensitivity reaches a maximum of 190°/RIU, but it falls short in detecting biomolecules with extremely low concentrations.

To boost the performance of the RI sensor, nine layers of BP are applied to the Ag layer in the conventional structure. Additionally, a 7-nm-thick silver layer is added to the top of the BP to mitigate oxidation in air. The results show that the sensitivity of the structure with 5.85-nm-thick BP and 7-nm-thick Ag is improved, as shown in Fig. 3b. The best sensitivity achieved is 340°/RIU. For further improvement, a $Ti_3C_2T_x$ layer with a thickness of 0.993 nm is coated on the 7-nm-thick Ag. The SPR resonance curve in Fig. 3c discloses a sensitivity as high as 450°/RIU.

The thickness of other materials is controlled, while the thickness of the first Ag layer is set to 30 nm, 35 nm, 40 nm, 45 nm, and 50 nm respectively. The sensitivities for the different Ag thicknesses are shown in Fig. 4. The results indicate that the sensitivity is the highest (450°/RIU) when the silver thickness is 40 nm.

The Ag coating with a thickness of 40 nm on black phosphorus as the third layer does not produce the surface plasmon resonance effects. Therefore, in order to increase the sensitivity, the thickness of the third Ag layer is optimized.

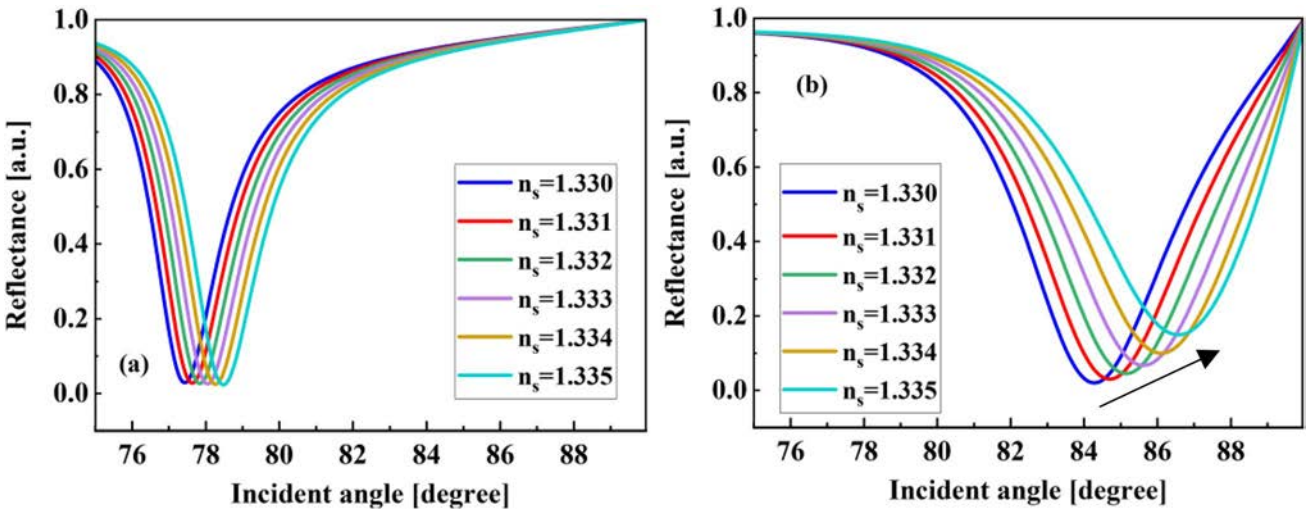

Fig. 6 **a** Variation of reflectance with respect to the incident angle for the refractive index range from 1.330 to 1.335 and **b** BP layers

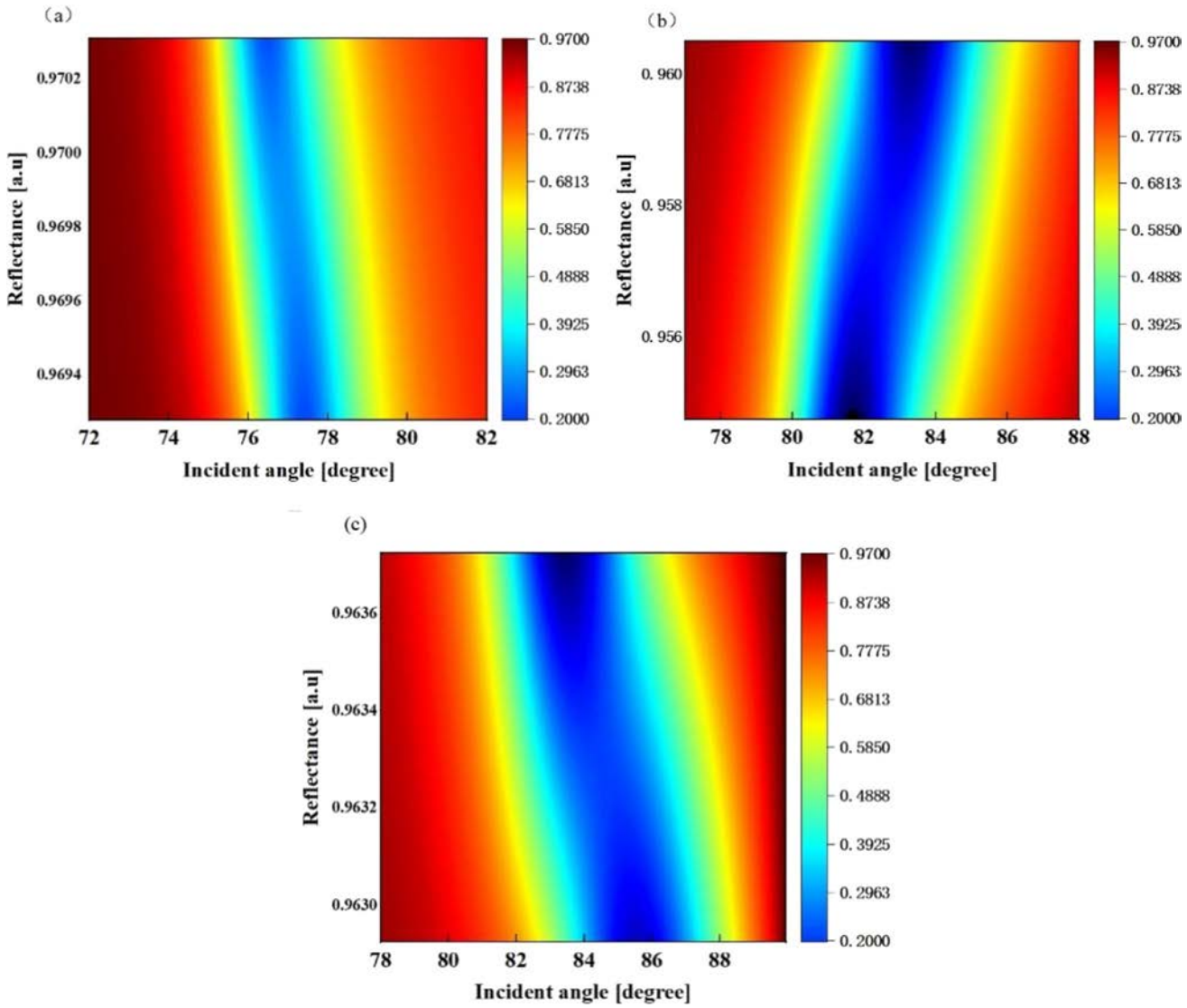

Fig. 7 Parametric contour plots: **a** CaF_2-Ag, **b** CaF_2-Ag-BP-Ag, and **c** CaF_2-Ag-BP-Ag-$Ti_3C_2T_x$

Table 2 Comparison of sensing performance at $\lambda = 662$ nm

Configuration (CaF_2 +)	$\Delta\theta_{SPR}$ (degree)	Sensitivity (°/RIU)	Analyte RI range ($n = 0.005$)
Ag	0.95	190	1.330 to 1.335
Ag + BP + Ag	1.70	340	1.330 to 1.335
Ag + BP + Ag + $Ti_3C_2T_x$	2.25	450	1.330 to 1.335

The sensitivity for different Ag thicknesses is shown in Fig. 5. The sensitivity increases as the thickness of the Ag layer increases, but the sensitivity decreases when the thickness exceeds 7 nm. The results show that the sensitivity is the highest (450°/RIU) when the silver thickness is 7 nm.

Figure 6a shows the responses of the structures with two-layer Ag and single-layer $Ti_3C_2T_x$, but without BP. Figure 6b shows the reflectance for different incidence angles of the structure

Table 3 Sensor structure with their computed performance factors

Configuration (CaF_2 +)	FWHM (degree)	DA (degree^{-1})	FOM (RIU^{-1})	DL ($\times 10^{-6}$)	SNR (dB)
Ag	2.89	0.346	65.74	2.38	0.48
Ag + BP + Ag	3.68	0.272	92.39	2.94	0.46
Ag + BP + Ag + $Ti_3C_2T_x$	4.35	0.23	103.45	5.26	0.33

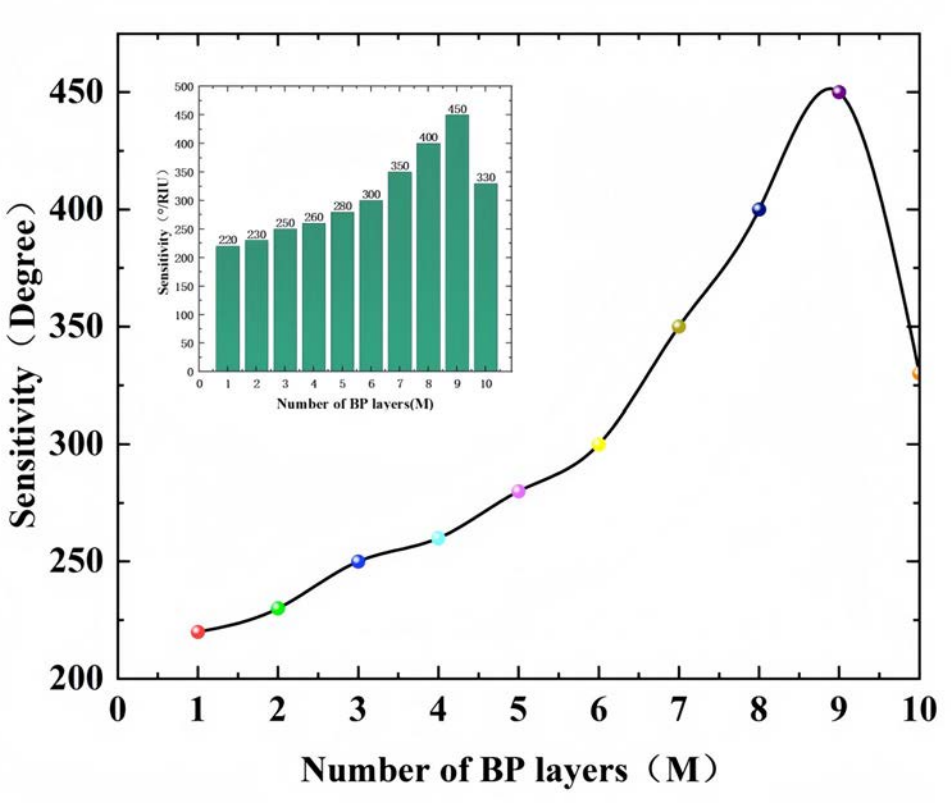

Fig. 8 Sensitivity of M = 9 and $N = 1$ for different refractive indexes

comprising Ag + BP + Ag + $Ti_3C_2T_x$ within the RI range from 1.330 to 1.335. The wave valley moves toward a larger incidence angle as the RI increases. The resonance angles are 84.3°, 84.7°, 85.15°, 85.6°, 86.1°, and 82.15° for $n_s = 1.330$, 1.331, 1.332, 1.333, 1.334, and 1.335, respectively. Figure 7 presents the contour diagrams illustrating the relationship between the incident angle and reflectance of the different structures.

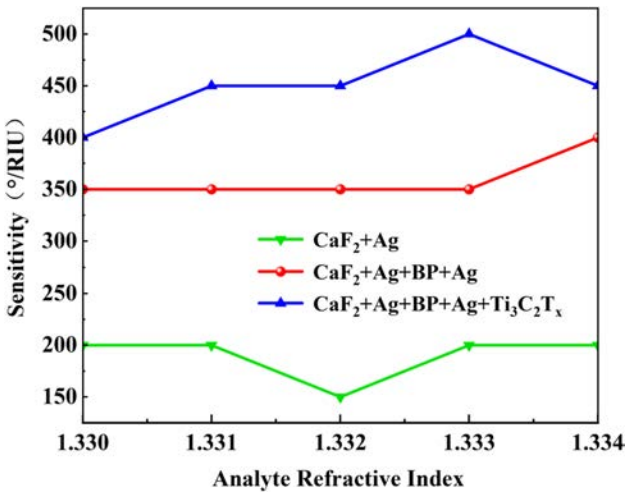

Fig. 9 Optimization of the sensitivity of different layer configurations for the RI range between 1.330 and 1.334 RIU

The sensitivities of conventional, bimetallic, and composite structures at a wavelength λ of 662 nm are shown in Table 2. The highest sensitivity of 450 (°/RIU) is achieved for the analyte RI change of $\Delta n_s = 0.001$. The structure (CaF_2 + Ag + BP + Ag + $Ti_3C_2T_x$) shows a shift in the resonance angle of $\Delta\theta_{SPR} = 2.25°$ when the analyte RI changes from 1.330 to 1.335, indicating that the sensitivity is indeed impacted by the layer number. The values computed for different performance factors are shown in Table 3.

To elucidate the physical mechanism between the number of black phosphorus layers and sensitivity, Fig. 8 shows the effects of the number of BP layers (M) with that of $Ti_3C_2T_x$ ($N = 1$) unchanged. The refractive index of the sensing medium is set to 1.33 + Δn. The sensitivity increases initially to a maximum of 450°/RIU when the number of BP layers is 9 (M = 9) but declines subsequently when M > 9.

Figure 9 shows the analysis for the RI range between 1.330 and 1.334. In the analysis, the sensitivity of a single layer of metallic silver is derived for different refractive indexes. The same is performed on the BP layer and titanium carbide layer, and the sensitivities are calculated separately. The sensitivity of the sensor increases gradually with the number of layers. Table 4 compares the performance of different sensors confirming the superiority of our sensor.

Table 4 Comparative analysis of sensitivity with relevant research work

References	Configuration	Sensitivity (°/RIU)	Structures
[1]	BP/Graphene/MoS_2 /WS_2/ $MoSe_2$/WSe_2	279	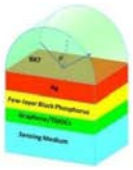
[4]	Cu/Ni/BP/MXene	304.4	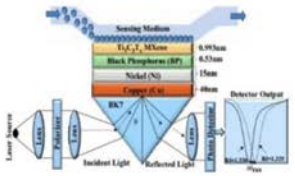
[2]	WS_2/$BaTiO_3$/BP	370	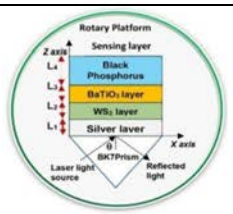
[3]	Prism/Ag/MXene/ Au/Graphene	301.2	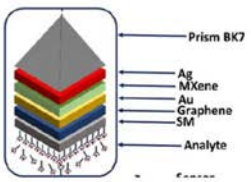
[45]	Prism/Au/BP/Au/S ensing Layer	218	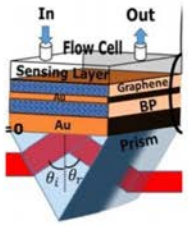
This work	CaF_2/Ag/BP/Ag/Ti_3 C_2T_x	450	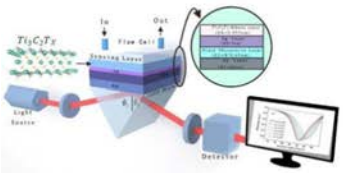

Conclusions

An SPR biochemical sensor composed of a CaF_2 prism, BP, MXene, and bimetallic Ag is designed to enhance the sensitivity. The sensitivity of the structure with silver coated on the CaF_2 prism is 190°/RIU. By introducing BP and another Ag layer, the sensitivity increases to 340°/RIU. When $Ti_3C_2T_x$ 2D is coated as a protective layer on the third Ag layer, the sensitivity is further improved. The heterostructure consisting of 0.993 nm-thick $Ti_3C_2T_x$ and BP shows the highest sensitivity of 450°/RIU. Compared to the conventional structure with one silver film, the sensitivity of the SPR comprising Ag, few-layer BP, and $Ti_3C_2T_x$ is improved by nearly 3.9 times. The results provide

insights into the design of high-performance SPR sensors for biochemical applications. In the future, SPR sensors will integrate a wide range of cutting-edge technologies, including computing, microfluidics, AI, and bioengineering, in order to improve their performance. Furthermore, the utilization of optical waveguide technology will enable the creation of efficient and miniature sensing elements, facilitating multi-sensor integration and further enhancing sensing capabilities.

Author Contributions A.Jingwei Lv: Conceptualization, Writing- Reviewing and Editing. B.Ying Yu: Conceptualization, Methodology, Software, Writing-Original Draft. C.Chao Mi: Investigation, Validation. D.Debao Wang: Formal analysis. E.Wei Li: Funding acquisition, Validation. F.Yanru Ren: Investigation. G.Jianxin Wang: Conceptualization. H.Wei Liu: Resources. I.Paul K. Chu: Project administration. J.Chao Liu: Resources, Writing- Reviewing and Editing. All authors reviewed the manuscript.

Funding This work was jointly supported by the National Natural Science Foundation of China (12304480), the Heilongjiang Provincial Natural Science Foundation of China (JQ2023F001), the Local Universities Reformation and Development Personnel Training Supporting Project from Central Authorities, Natural Science Foundation of Heilongjiang Province (LH2021F007), the China Postdoctoral Science Foundation–funded project (2020M670881), the Study Abroad returnees merit-based Aid Foundation in Heilongjiang Province (070–719900103), the City University of Hong Kong Strategic Research Grant (SRG) (7005505), and the City University of Hong Kong Donation Research Grants (DON-RMG 9229021 and 9220061).

Data Availability No datasets were generated or analysed during the current study.

Declarations

Competing Interests The authors declare no competing interests.

References

1. Wu L et al (2017) Sensitivity enhancement by using few-layer black phosphorus-graphene/TMDCs heterostructure in surface plasmon resonance biochemical sensor. Sens Actuators, B Chem 249:542–548
2. Srivastava A, Das R, Prajapati YK (2020) Effect of perovskite material on performance of surface plasmon resonance biosensor. IET Optoelectron 14(5):256–265
3. Karki B et al (2024) Tuning sensitivity of bimetallic, MXene and graphene-based SPR biosensors for rapid malaria detection: a numerical approach. J Comput Electron 23： 920–929
4. Kumar R et al (2021) High-performance bimetallic surface plasmon resonance biochemical sensor using a black phosphorus–MXene hybrid structure. Appl Phys A 127(4):259
5. Liu J et al (2020) Are plasmonic optical biosensors ready for use in point-of-need applications? Analyst 145(2):364–384
6. Homola J (2008) Surface plasmon resonance sensors for detection of chemical and biological species. Chem Rev 108(2):462–493
7. Wang J et al (2019) Surface plasmon resonance sensor for low refractive index detection based on microstructured fiber. JOSA B 36(11):3104–3110
8. Pandey AK (2021) Graphene–Ti3C2Tx MXene hybrid nanostructure: a promising material for sensitivity enhancement in plasmonic sensor. Appl Phys A 127.2:78
9. Chen S, Lin C (2019) Sensitivity analysis of graphene multilayer based surface plasmon resonance biosensor in the ultraviolet, visible and infrared regions. Appl Phys A 125:1–6
10. Dyr JE et al (1998) Molecular arrangement of adsorbed fibrinogen molecules characterized by specific monoclonal antibodies and a surface plasmon resonance sensor. Sens Actuators B Chem 51(1–3):268–272
11. Maurya JB, Prajapati YK (2016) A comparative study of different metal and prism in the surface plasmon resonance biosensor having MoS 2-graphene. Opt Quant Electron 48:1–12
12. Sharma AK, Gupta BD (2007) On the performance of different bimetallic combinations in surface plasmon resonance based fiber optic sensors. J Appl Phys 101(9): 093111
13. Shukla S, Sharma NK, Sajal V (2016) Theoretical study of surface plasmon resonance-based fiber optic sensor utilizing cobalt and nickel films. Braz J Phys 46:288–293
14. Kumar Maharana P, Bharadwaj S, Jha R (2013) Electric field enhancement in surface plasmon resonance bimetallic configuration based on chalcogenide prism. J Appl Phys 114(1): 014304
15. Churchill HO, Jarillo-Herrero P (2014) Phosphorus joins the family. Nat Nanotechnol 9(5):330–331
16. Li L et al (2014) Black phosphorus field-effect transistors. Nat Nanotechnol 9(5):372–377
17. Rodin AS, Carvalho A, Castro Neto AH (2014) Strain-induced gap modification in black phosphorus. Phys Rev Let 112(17):176801
18. Wang L, Tian SC, Li L (2014) Research on evaluation index system of safety culture construction in oilfield teams. 2014 7th international conference on intelligent computation technology and automation. IEEE 517-521
19. Srivastava A, Prajapati YK (2019) Performance analysis of silicon and blue phosphorene/MoS 2 hetero-structure based SPR sensor. Photonic Sens 9:284–292
20. Singh Y, Raghuwanshi SK (2019) Sensitivity enhancement of the surface plasmon resonance gas sensor with black phosphorus. IEEE Sens Lett 3(12):1–4
21. Malitson IH (1963) A redetermination of some optical properties of calcium fluoride. Appl Opt 2(11):1103–1107
22. Hossain B et al (2022) A highly sensitive surface plasmon resonance biosensor using SnSe allotrope and heterostructure of BlueP/MoS2 for cancerous cell detection. Optik 252:168506
23. Pandey PS, Raghuwanshi SK, Singh Y (2022) Enhancement of the sensitivity of a surface plasmon resonance sensor using a nobel structure based on barium titanate–graphene-silver. Opt Quantum Electron 54(7):417
24. Castellanos-Gomez A (2015) Black phosphorus: narrow gap, wide applications. The journal of physical chemistry letters 6(21):4280–4291
25. Walia S et al (2016) Defining the role of humidity in the ambient degradation of few-layer black phosphorus. 2D Mat 4(1):015025
26. Pal S et al (2017) Influence of black phosphorous on performance of surface plasmon resonance biosensor. Opt Quantum Electron 49:1–13
27. Pal S et al (2020) Sensitive detection using heterostructure of black phosphorus, transition metal di-chalcogenides and MXene in SPR sensor. Appl Phys A 126(10):809
28. Wu Q et al (2019) A 2D transition metal carbide MXene-based SPR biosensor for ultrasensitive carcinoembryonic antigen detection. Biosens Bioelectron 144:111697
29. Xin M et al (2020) MXenes and their applications in wearable sensors. Front Chem 8:297
30. Wang Z et al (2020) Recent advances in MXenes composites for electromagnetic interference shielding and microwave absorption. Compos Part A Appl Sci Manuf 136:105956

31. Khazaei M et al (2013) Novel electronic and magnetic properties of two-dimensional transition metal carbides and nitrides. Adv Funct Mat 23(17):2185–2192
32. Lin H et al (2017) Two-dimensional ultrathin MXene ceramic nanosheets for photothermal conversion. Nano Lett 17(1):384–391
33. Naguib M et al (2011) Two-dimensional nanocrystals produced by exfoliation of Ti3AlC2. Adv Mater 23:4248–4253
34. Sinha A et al (2018) MXene: An emerging material for sensing and biosensing. TrAC Trends Anal Chem 105:424–435
35. Zheng J et al (2018) Synthesis of MXene/DNA/Pd/Pt nanocomposite for sensitive detection of dopamine. J Electroanal Chem 816:189–194
36. Wang F et al (2015) TiO2 nanoparticle modified organ-like Ti3C2 MXene nanocomposite encapsulating hemoglobin for a mediator-free biosensor with excellent performances. Biosens Bioelectron 74:1022–1028
37. Lorencova L et al (2017) Electrochemical performance of Ti3C2Tx MXene in aqueous media: towards ultrasensitive H2O2 sensing. Electrochim Acta 235:471–479
38. Gupta BD, Sharma AK (2005) Sensitivity evaluation of a multi-layered surface plasmon resonance based fiber optic sensor: A theoretical study. Sens Actuators B Chem 107(1):40–46
39. Kumar R et al (2020) Effect of silicon on sensitivity of SPR biosensor using hybrid nanostructure of black phosphorus and MXene. Superlattices Microstruct 145:106591
40. Paswan MK, Basu R (2024) Hybrid structure–based SPR sensor for chemical sensing with enhanced sensitivity. Plasmonics 19(2):765–776
41. Pandey PS, Raghuwanshi SK (2022) Sensitivity enhancement of surface plasmon resonance (SPR) sensor assisted by BlueP/MoS 2 based composite heterostructure. IEEE Access 10:116152–116159
42. Miranda A et al (2017) Rendering Ti3C2T x (MXene) monolayers visible. Mat Res Lett 5(5):322–328
43. Lin Z et al (2016) Tuning and sensitivity enhancement of surface plasmon resonance biosensor with graphene covered Au-MoS 2-Au films. IEEE Photonics J 8(6):1–8
44. Singh Y, Paswan MK, Raghuwanshi SK (2021) Sensitivity enhancement of SPR sensor with the black phosphorus and graphene with bi-layer of gold for chemical sensing. Plasmonics 16:1781–1790
45. Wu L, Jia Y, Jiang L, Guo J, Dai X, Xiang Y, Fan D (2017) Sensitivity improved SPR biosensor based on the MoS2/graphene-aluminum hybrid structure. J Lightwave Technol 35(1):82–87
46. Masson J-F (2017) Surface plasmon resonance clinical biosensors for medical diagnostics. ACS sensors 2(1):16–30
47. Luo X et al (2024) High-sensitivity dual U-shaped PCF-SPR refractive index sensor for the detection of gas and liquid analytes. JOSA A 41(4):595–605
48. Mudgal N et al (2022) Impact of Taguchi optimization in fiber surface plasmon resonance sensors based on Si3N4 Layer. Braz J Phys 52(3):80
49. Mudgal N et al (2020) BaTiO 3-graphene-affinity layer–based surface plasmon resonance (SPR) biosensor for pseudomonas bacterial detection. Plasmonics 15:1221–1229
50. Karki B et al (2024) Tuning sensitivity of surface plasmon resonance gas sensor based on multilayer black phosphorous. Modern Phys Lett B 14:2450364
51. Hma Salah N, Pal A, Uniyal A (2024) Enhancing precision in fuel adulteration detection: Utilizing a wavelengthinterrogation surface plasmon resonance approach. Plasmonics 1–10
52. Aliqab K et al (2023) A theoretical analysis of refractive index sensor with improved sensitivity using titanium dioxide, graphene, and antimonene grating: Pseudomonas bacteria detection. Measurement 216:112957